frontiers in Chemical Engineering

ORIGINAL RESEARCH
published: 16 November 2020
doi: 10.3389/fceng.2020.589686

A 3D-Printed Zeolitic Imidazolate Framework-8 Monolith For Flue- and Biogas Separations by Adsorption: Influence of Flow Distribution and Process Parameters

*Brieuc Verougstraete[1], Dieter Schuddinck[1], Jasper Lefevere[2], Gino V. Baron[1] and Joeri F. M. Denayer[1]**

[1] Department of Chemical Engineering, Vrije Universiteit Brussel, Brussels, Belgium, [2] Vlaams Insitituut voor Technologische Ontwikkeling (VITO NV), Mol, Belgium

Improving the efficiency of gas separation processes for CO_2 capture is primordial. In the field of adsorptive separation processes, a shift to structured adsorbents, more especially monoliths, can be seen. These offer better efficiency, better mass transfer characteristics and a lower pressure drop compared to the conventional shape of adsorbents. This could lead to short adsorption/desorption cycles, which is crucial. In this study we analyzed a 3D-fiber deposited zeolitic imidazolate framework (ZIF)-8 monolith. The resulting interwoven structure of the monolith has the advantage to allow for radial diffusion in between the channels. Therefore, the gas flow distribution inside the monolith was investigated. This was done experimentally, but also *in silico*. Next, breakthrough experiments were performed to study the influence of flow rate and desorption time, since ZIF-8 can easily be regenerated. It was seen that flowing air through the monolith for 6 s was sufficient to regenerate the monolith. Regarding the hydrophobicity of ZIF-8, the presence of water vapor in the gas stream was investigated. Lastly, the separation factor of ZIF-8 for CO_2 over CH_4 was determined.

Keywords: zeolitic imidazolate framework-8, 3D-printed, monolith, adsorption, CO_2

OPEN ACCESS

Edited by:
Alessio Caravella, Università della Calabria, Italy

Reviewed by:
Grazia Leonzio, Imperial College London, United Kingdom
Pasquale Francesco Zito, Italian National Research Council, Italy

****Correspondence:***
Joeri F. M. Denayer
Joeri.denayer@vub.be

Specialty section:
This article was submitted to Separation Processes, a section of the journal Frontiers in Chemical Engineering

Received: *11 August 2020*
Accepted: *30 September 2020*
Published: *16 November 2020*

Citation:
Verougstraete B, Schuddinck D, Lefevere J, Baron GV and Denayer JFM (2020) A 3D-Printed Zeolitic Imidazolate Framework-8 Monolith For Flue- and Biogas Separations by Adsorption: Influence of Flow Distribution and Process Parameters. Front. Chem. Eng. 2:589686. doi: 10.3389/fceng.2020.589686

INTRODUCTION

Over the last years, an increasing interest in structured adsorbents, and more specifically monoliths, can be noticed. Compared to conventionally shaped adsorbents like beads or pellets, these structures lead to lower pressure drop and an improved mass and heat transfer (Avila et al., 2005; Rezaei and Webley, 2009; Rezaei and Webley, 2010; Rezaei and Grahn, 2012; Hasan et al., 2013). As a result, they allow higher gas velocities and can thus lead to much shorter cycle times in an adsorption/desorption cycle. Due to the need for short cycles in the field of CO_2 capture, monolithic structures are becoming more important (Hasan et al., 2013; Middelkoop et al., 2019). To prepare these monoliths, traditional methods consist of coating a support monolith with the adsorbent or directly by extrusion (Williams, 2001; Avila et al., 2005; Akhtar et al., 2014; Govender and Friedrich, 2017). When using coating techniques, a monolithic support will be used on which a film of active material will be deposited, implying that a major part of the structure will not contribute to the adsorption capacity. For the

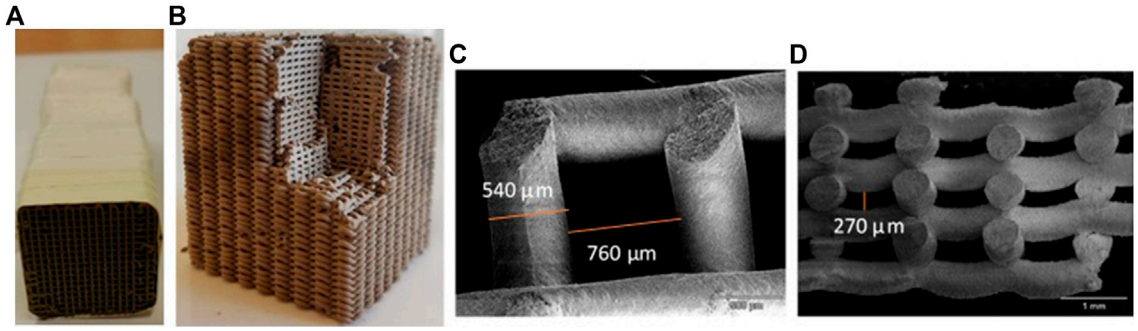

FIGURE 1 | Picture of 3DFD-printed zeolitic imidazolate framework-8 Monolith. **(A)** Monolith used for breakthrough experiments. Several pieces were stacked and held together with Teflon tape. **(B)** Side view showing the presence of channels in the radial direction. **(C)** Scanning electron microscopy-picture of the top-view of the monolith. **(D)** Scanning electron microscopy-picture of side view visualizing the radial gaps present in the structure.

extrusion process, the paste will pass through a die, which is expensive to produce and limits the structures that can be obtained. For lab scale experimentation and evaluation of new structures, these disadvantages can be overcome by an emerging technique, namely 3D-printing, also called additive manufacturing. Using this technique, a variety of structures that are complex or impossible to produce with traditional methods, are made available (Lee et al., 2017; Ruiz-Morales et al., 2017).

In recent years, several publications on 3D-printed adsorbent for CO_2 capture have been issued, demonstrating the growing interest in this field. Couck et al. (2017) and Couck et al. (2018) reported 3D-printed monolithic structures based on ZSM-5 and SAPO-34 zeolites for the separation of CO_2 from N_2 and/or CH_4. Thakkar et al. (2018) reported the performance of 5A and 13× based monolithic adsorbent. Also, hybrid 3D-printed structures containing activated carbon and zeolite for CO_2 capture using electrical swing adsorption are reported (Regufe et al., 2019). This shows the heterogeneity in materials that can be utilized using the 3D-printing technique.

An alternative class of material that can be used for gas separation are zeolitic imidazolate frameworks (ZIFs), with mainly the focus on ZIF-8. ZIF-8 is one of the most studied MOFs since it is easy to produce and exhibits a high thermal and chemical stability, a high surface area and a good hydrophobicity, which facilitates the regeneration step (Park et al., 2006; Küsgens et al., 2009; McEwen et al., 2013). This water stability is also advantageous as flue gases and biogas mixtures contain water vapor (Zhang et al., 2011).

Most of the studies discussing CO_2 adsorption with ZIF-8 are focusing on the higher pressure range. However, Huang et al. (2011) studied the effect of temperature on adsorption of CO_2, CH_4 and N_2 in pure gas adsorption and for gas mixtures. McEwen et al. (2013) compared the adsorption isotherms for N_2, CH_4 and CO_2 on ZIF-8 in a range from 0 to 1 bar, showing that ZIF-8 preferentially adsorbs CO_2 over CH_4. Various studies studied this in more detail (Venna and Carreon, 2010; Autié Castro et al., 2017).

In this work, a 3D-printed fiber deposited ZIF-8 monolith was studied for the separation of CO_2. The effect of the 3DFD-technique on the gas distribution inside the monolith was assessed since the 3D-printing method applied here results in radial gaps in the structure. The possible impact of selected process parameters was evaluated in dynamic conditions. Lastly, the separation factor between CO_2 and CH_4 was assessed.

MATERIALS AND METHODS

Material Properties

The synthesis of the 3D-printed ZIF-8 monolith and its performance in the adsorption of butanol has already been published in earlier work (Lefevere et al., 2019; Claessens et al., 2020). The monolithic adsorbent was supplied by VITO and produced using a 3D-printing fiber deposition method (**Figure 1**). The different constituents to produce the monolith were ZIF-8 powder (66.7 wt%) (Basolite 1200, Sigma-Aldrich), bentonite (16.7 wt%) (VWR) and methylcellulose (16.7 wt%) (Acros organics) which were mixed with water to form a printable paste. After activation under Argon at 450°C, resulting in the removal of the methylcellulose, a final composition of 80 wt % ZIF-8 and 20 wt% bentonite was obtained.

Due to limitations in the 3D-printing process, several individual 3D-printed monoliths with a length between 2.0 and 2.9 cm and width between 2.3 and 2.5 cm were stacked to obtain an adsorbent with a final length of 11.5 cm and a mass of 17.61 g. The fibers, extruded using a nozzle of 600 μm, had a diameter of 540 μm. The channel size was equal to 760 μm. The average number of channels per block was 18 × 18. As a result of the fiber deposition method, side channels of ~270 μm are seen (**Figure 1D**). The external porosity was calculated by dividing the volume of the channels by the total volume and was equal to 0.58.

Scanning electron microscopy images were taken with a JEOL device (JSM-6400) under vacuum, using an acceleration voltage of 5 kV.

$CO_2/CH_4/N_2$ isotherms were measured using an Autosorb-1 (Quantachrome Instruments, Odelzhausen, Germany) device. Regeneration of the samples was done by outgassing at 150°C for 180 min. Isotherms were measured at 25, 50, and 70°C for all three gases. To gain a better insight on the meso- and macroporosity in the fibers, the structure was analyzed using

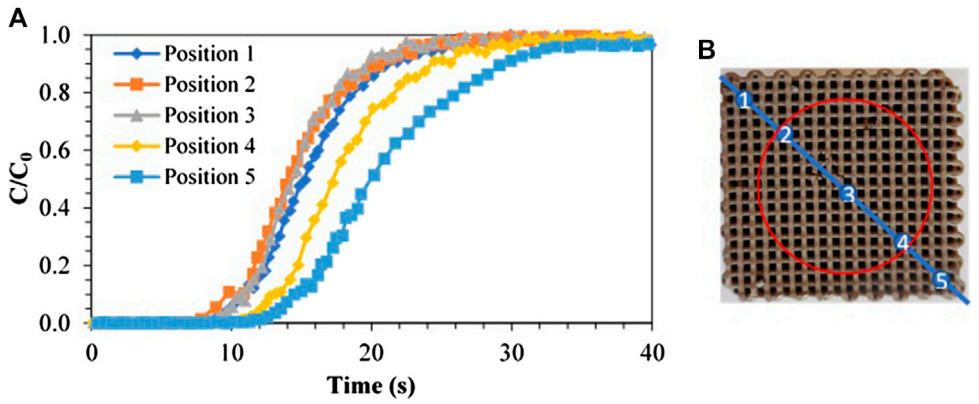

FIGURE 2 | Breakthrough curves obtained in different radial positions. **(A)** Breakthrough curve in the five different radial positions along the diagonal. **(B)** Scheme of the diagonal and the positions at which the breakthrough profile was measured. The red circle shows the size of the inlet.

Hg-porosimetry (Pascal Mercury Porosimeters, Thermo Scientific). From these measurements, the mean pore diameter was calculated to be 0.37 μm. Complete data on the pore volume can be found in previous work (Lefevere et al., 2019; Claessens et al., 2020). A water adsorption isotherm was determined at 25°C by means of a gravimetric technique (VTI, TA Instruments, New Castle, PA).

Dynamic Separation Experiments

Cyclic breakthrough experiments were performed on an in-house built system. A detailed description of this setup can be found in earlier work (Verougstraete et al., 2020). To connect the monolith with the setup, a 3D-printed gas inlet was designed in polylactic acid (Ultimaker 3, Delgermalsen, The Netherlands). The diameter of this inlet was 1.8 cm. Between the inlet and the monolith, a dead space of 0.1 cm was used for better dispersion of the gas.

The experimental setup allowed for high gas velocities inside the structured adsorbent. Therefore, gas velocities between 4.45 and 89.06 cm/s, corresponding with contact times of respectively 2.58 and 0.13 s, were used during adsorption. The synthetic gas mixture was made with CO_2 and/or CH_4 which was then diluted in pressurized air (~78% N_2, 21% O_2 and 1% Ar). To this stream, evaporated water could be added. In the next step, regeneration of the ZIF-8 monolith was done using compressed air at a high flow rate (10.0 Nl/min).

The adsorbed amount of CO_2 was calculated after a full breakthrough by the next equation (**Eq. 1**):

$$q = \frac{(\tau - t_d) \times F_{\text{ads}}}{m \times V_m}$$

With q the adsorption capacity (mmol/g), τ and t_d respectively the breakthrough time and the dead time of the setup (min), F_{ads} the flow rate of the pure adsorbate (Nl/min), m_{mon} the mass of the adsorbent (g) and V_m the molar volume (L/mmol). Note that every breakthrough experiment was performed twice to reduce manual errors in the measurements.

To gain a better insight into the breakthrough experiments and the flow profile inside the 3D-printed structure with radial gaps, an *in silico* study was performed to study the flow pattern inside the monolith using the Fluent console of Ansys.

For biogas separation, the efficiency of the separation was estimated by the separation factor α of CO_2 over CH_4, which was calculated for different compositions of feed gases (**Eq. 2**):

$$\alpha_{CO_2/CH_4} = \frac{q_{CO_2}}{q_{CH_4}} \times \frac{P_{CH_4}}{P_{CO_2}}$$

RESULTS AND DISCUSSION

Study at Different Radial Positions

Firstly, breakthrough experiments with a gas mixture containing 15 v% CO_2–85 v% air were performed. **Figure 2** represents the breakthrough curves of five identical experiments at room temperature, with a flow rate of 1.0 Nl/min, each measured at the outlet of the monolith but at different radial positions (**Figure 2B**). The aim was to study the impact of a smaller inlet diameter (1.8 cm)—represented with a red circle in **Figure 2B** compared to the size of the monolith (2.3 cm width), normally leading to a flow maldistribution in typical monoliths. However, since the fiber deposition method was used to 3D-print the monolith, radial gaps between the channels were present and radial diffusion between the channels occurs (**Figures 1B,D**). In **Figure 2A**, when looking at positions 1–3 or 3–5, a trend toward faster breakthrough of the monolith in the center can be noticed. However, the trend is different in both directions away from the center. Between positions 3 and 1, a difference of 12.6% in adsorption capacity was calculated (0.083 vs. 0.095 mmol/g), which can be perceived by a small deviation in the breakthrough curves, while a difference of 34.1% was calculated between positions 3 and 5 (0.083 vs. 0.126 mmol/g). Normally, positions 1 and 2 should result in the same breakthrough curve as positions 4 and 5 respectively as they are equally distant to the center of the monolith. These inhomogeneous breakthrough curves are partially due to the stacking of the different blocks of ZIF-8 monolith with a different width together, which engender some channels to be

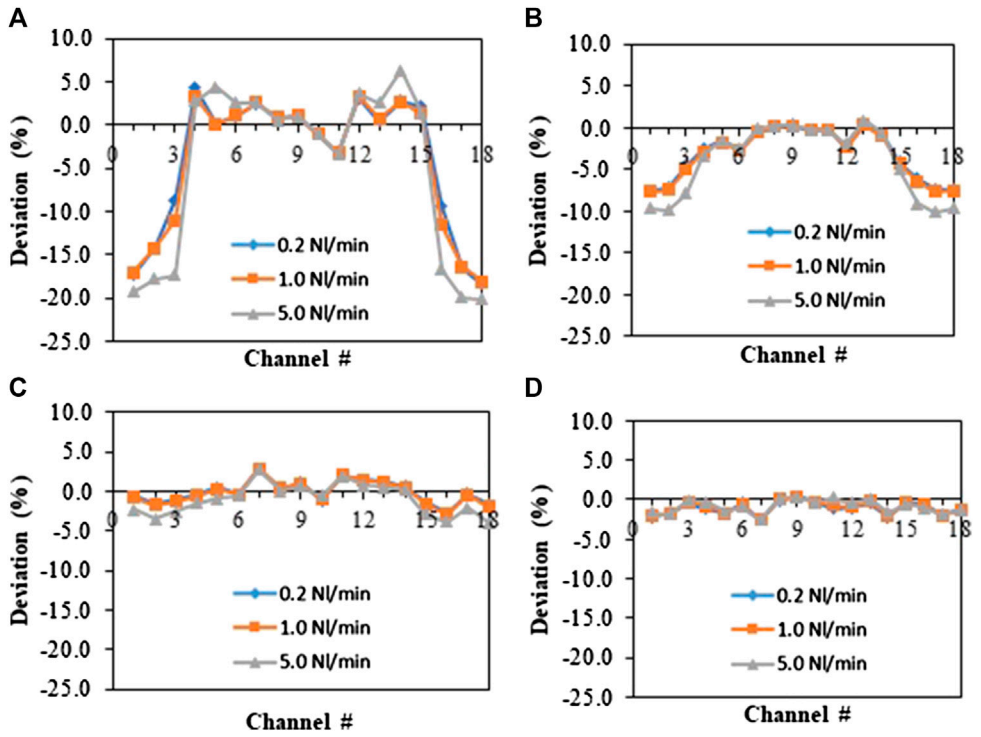

FIGURE 3 | Deviation of the maximal longitudinal velocity in each channel relative to the middle channels (Channels 9 and 10) at different axial positions inside the monolithic structure in the reference situation. **(A)** 0.1 cm, **(B)** 0.5 cm, **(C)** 1 cm, and **(D)** 2 cm; Flow rates of 0.2 Nl/min (blue), 1 Nl/min (orange), 5 Nl/min (gray).

hindered, resulting in flow maldistribution and the formation of dead volumes inside the adsorbent. Moreover, due to a limited mechanical strength of the material, the monolith was partly internally damaged which probably caused the blocking of some channels. In any case, these data show that imperfections in the structure result in the spreading of the overall concentration profile, as the resulting breakthrough curve (for the entire monolith) corresponds to the summation of all individual breakthrough curves from the different channels in the structure.

To gain a better knowledge of the flow distribution inside the monolith, a reference situation was simulated. The cylindrical feed inlet was followed by the monolithic structure with an empty space of 0.1 cm between them. Gas flow rates of 0.2, 1.0 and 5.0 Nl/min were simulated. **Figure 3** reflects the deviation of the maximal velocity inside each channel (along the diagonal) from the maximal velocity in the central channel at different axial positions (0.1, 0.5, 1, and 2 cm from the inlet) for the different flow rates. Close to the inlet, strong deviations (up to 20%) in the maximal velocities were observed (**Figure 3A**). **Figure 3B** indicates that after 0.5 cm inside the monolith, the deviations in velocities are already more than halved and they continue to flatten out afterward due to the woven structure. At distances of 1 or 2 cm from the inlet, somewhat higher velocities are still found at the center, which still indicates a small flow maldistribution, but the deviations in velocities are small (below 3%). This indicates that in the monolith used for the experiments, the gas will be rapidly well distributed over the whole cross-section. Adsorption was not taken into account in the simulation, but the results of the flow distribution suggest that the deviations seen in the experiments are only minorly caused by flow maldistribution, which highlights the importance of issues of joining and collapsing of the monolith. To limit these issues in further experiments and to obtain consequent results, concentration profiles were all measured in the central channel (Position 3) in subsequent experiments.

CO_2 Isotherm

Figure 4 shows the pure component adsorption isotherms of CO_2 obtained on a fragment of the monolith in static conditions (volumetric analysis). This test was repeated multiple times. Surprisingly, the shape of the isotherm is different from the linear isotherm found for ZIF-8 in the low pressure range in the literature (Huang et al., 2011; McEwen et al., 2013). The adsorption capacity obtained at 1 bar is also higher than the capacity reported in the literature (1.30 mmol/g instead of 0.82 mmol/g). A separate test was performed on the ZIF-8 powder used to fabricate the monolith, to evaluate if this change could be linked to the binder or to the 3D-printing technique. A similar adsorption isotherm was obtained, showing the very limited impact of bentonite on the capacity. An additional CO_2 isotherm on ZIF-8 powder from BASF was measured for comparison with literature (**Figure S1**). Again, the same isotherm was obtained.

Next, a CO_2-isotherm (at 25°C) was measured in dynamic conditions, thus under flow, on the breakthrough setup. The flow rate was 1 Nl/min for all experiments and consisted of a dry gas mixture of compressed air and CO_2. Measurements were performed using 5, 10, 15, 25, 50, 75, and 100 v% CO_2. In

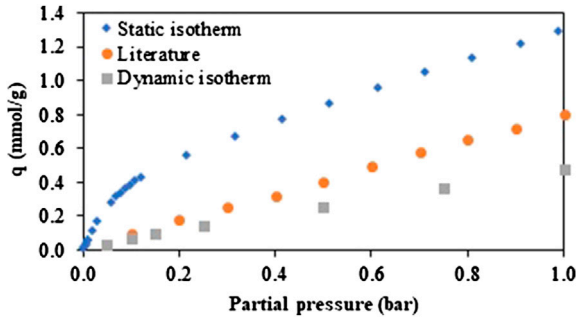

FIGURE 4 | Comparison of CO_2-isotherms on zeolitic imidazolate framework-8 at 25°C. Isotherm measured under static conditions (blue), isotherm reported in literature (McEwen et al., 2013) (orange) and isotherm measured under dynamic conditions for 5, 10, 15, 25, 50, 75, and 100 v% of CO_2 (1 Nl/min.) (gray).

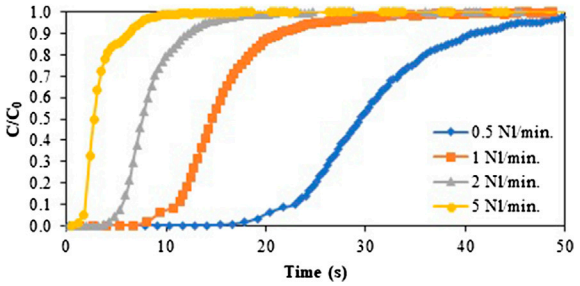

FIGURE 5 | Normalized breakthrough curves at different adsorption flow rates. 0.5 Nl/min (blue), 1 Nl/min (orange), 2 Nl/min (gray) and 5 Nl/min (yellow). Adsorption was performed at room temperature (25°C) and using a feed gas containing 15 v% CO_2.

Figure 4, it can be seen that the isotherm measured in dynamic conditions is linear, like the static isotherm from the literature. Also, the capacity is much lower than in static conditions, especially in the low-pressure region. Several effects can be at the basis of this discrepancy. First, the CO_2-isotherm measured in dynamic conditions was obtained in presence of N_2, since air is added to the mixture. However, the pure component isotherm of N_2 (**Figure S2**) shows that the amount of CO_2 adsorbed is at least 15 times larger than that of N_2 at the same partial pressure (below 1 bar), therefore this will only have a limited effect. Secondly, there is a small heat effect caused by the exothermic nature of adsorption of CO2, which will increase the temperature in the monolith. As experimentally determined, the temperature gain was limited to 2°C for a gas with 15 v% CO2, but this will still slightly reduce the capacity. However, isotherms measured at different temperatures show that, at low partial pressure, the effect of temperature is rather small (**Figure S3**). Moreover, to limit the impact of the heat, the breakthrough time was taken long enough as for the monolith to reach (almost) its initial temperature. Thirdly, possibly no complete equilibrium is obtained in dynamic conditions due to diffusion limitations, but the presence of a large fraction of macropores, as evidenced by Hg-porosimetry, indicates that a rather fast diffusion should occur (**Figure S4**).

Another possible explanation for the major difference between the dynamic and the static isotherm, is that for the latter, material activation (at 150°C) was combined with outgassing at a deep vacuum ($<1 \times 10^{-6}$ bar) during a long time (>3 h). For the dynamic isotherm, no vacuum conditions were applied. This more severe activation could liberate more adsorption sites or even result in a modified pore structure; it is well known that twisting of the ligands in the ZIF-8 structure under certain conditions impacts the adsorption capacity due to a deformation of the ZIF-8 framework (Fairen-Jimenez et al., 2011; Fairen-Jimenez et al., 2012; Tanaka et al., 2015; Coudert, 2017). These additional sites will fill already at low partial pressures and from a partial pressure of 0.2 bar, the shape of the isotherm becomes linear. Moreover, the static isotherm is then approximatively parallel to the one reported, meaning that the difference will be similar. The data points measured for the dynamic isotherm were obtained after a regeneration that did not involve a deep vacuum, therefore lower capacities are obtained.

Effect of Flow Rate

The effect of gas velocity on the adsorption capacity was studied in breakthrough experiments to further investigate and identify possible mass transport limitations (**Figure 5**). This was performed using a fixed feed gas mixture (15 v% CO_2 and 85 v % air). Breakthrough curves were measured at four different flow rates, namely 0.5, 1.0, 2.0, and 5.0 Nl/min, which corresponds to gas velocities between 0.045 and 0.89 m/s. These high velocities lead to a reduced contact time between the CO_2 molecules and the structured adsorbent, ranging from 0.13 to 2.58 s. Even at very high flow rates, a typical S-shaped curve is obtained. The adsorption capacities calculated from these breakthrough experiments were constant (~0.088 mmol/g). This enhances the theory that the low capacity values obtained for the dynamic isotherm are not due to a limitation in diffusion. Note that a discontinuity at the beginning of the curves is observed for the two lowest flow rates, corresponding to an early breakthrough caused by flow maldistribution and by-passing.

Effect of Desorption Time on the Cyclic Performance

A study was performed to determine how efficiently CO_2 can be desorbed from the ZIF-8 monolith at ambient temperature by purging with air (10 Nl/min). Consecutive adsorption/desorption cycles were performed while decreasing the desorption time. **Figure 6A** shows the effect of desorption time on cyclic capacity. Since the adsorption capacity matched the base case scenario after a thermal regeneration at a desorption time of 20 s, desorption times in the range of 3–20 s were evaluated. When reducing the regeneration time till 6 s, still no significant effect on the adsorption capacity can be noted. This means that, even if the cyclic adsorption capacity of the 3D-printed monolith is rather low, it can be regenerated very rapidly in isothermal conditions. At even lower desorption time (<6 s), not all CO_2 is desorbed, resulting in a decrease of the cyclic adsorption capacity. This can

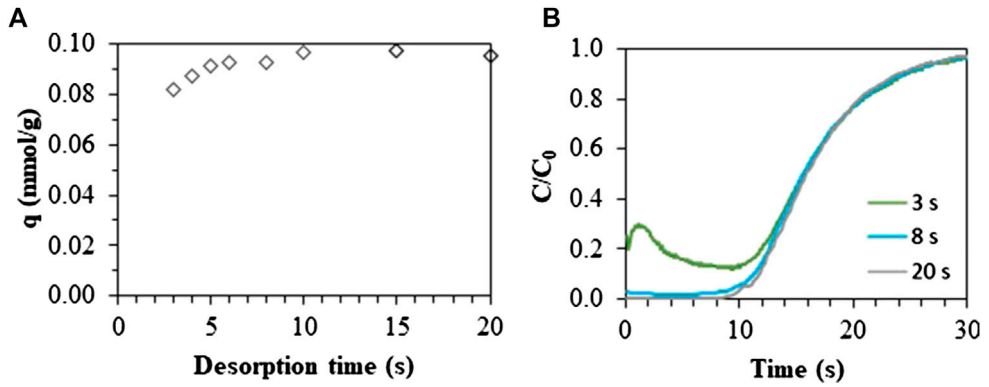

FIGURE 6 | Adsorption capacities for different desorption times at a desorption flow rate of 10 Nl/min. Adsorption was performed at a flow rate of 1 Nl/min (15 v% CO_2, 85 v% air) during 100 s at 26°C. **(A)** Adsorption capacities for a desorption time in the range of 3–20 s. **(B)** Normalized breakthrough curve measured after a regeneration time of 3 s (green), 8 s (light blue) and 20 s (gray).

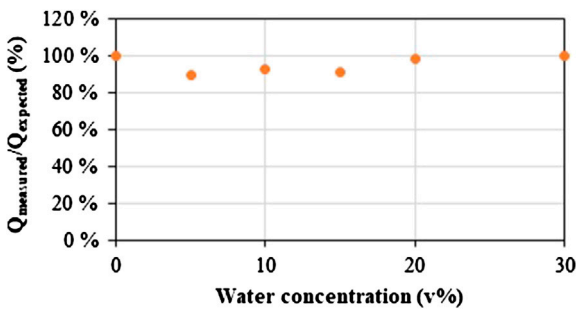

FIGURE 7 | Ratio of the adsorption capacity calculated from the breakthrough curve divided by the adsorption capacity expected for a specific relative pressure of CO_2 from the dynamic isotherm (**Figure 4**) in function of a different water concentration in the feed stream (More details in **Supplementary Material**).

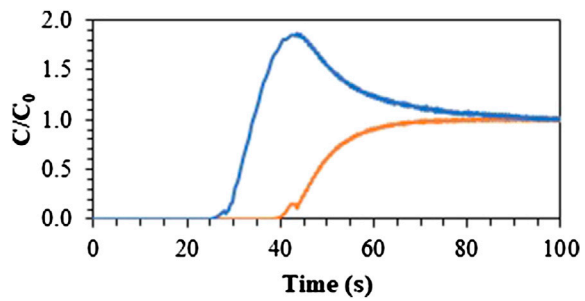

FIGURE 8 | Breakthrough curves at 26°C for separation of household waste stream biogas (60 v% CH_4, 33 v% CO_2, 7 v% air –0.5 Nl/min). CH_4 (Blue) and CO_2 (Orange).

be understood by evaluating the breakthrough curve obtained after regeneration using different desorption times (**Figure 6B**). For desorption times of 8 and 20 s, the concentration in the breakthrough curve remains zero in an initial period of the desorption step. However, at a desorption time of 3 s, a limited amount of CO_2 is still present in the material near the end of the column due to insufficient regeneration. When starting adsorption in co-current mode, this CO_2, near the column outlet, elutes immediately at the start of the adsorption step, which explains the bump in the breakthrough curve. It can be noticed that after this initial period, the curve increases similar to the other curves since the CO_2 was displaced and therefore breakthrough occurred at the same time. As mentioned in previous work, better performance is to be expected when regeneration is performed in counter-current mode (Verougstraete et al., 2020).

Effect of Water Content in Gas Stream

Since most of the targeted CO_2 mixtures (flue gas, biogas) for gas separation contain a certain amount of water, the effect of humidity in the feed gas was investigated. ZIF-8 is a very hydrophobic material, which is confirmed by the water isotherm measured on the 3D-printed ZIF-8 sample (**Figure S5**). Therefore, only a small effect of water on the adsorption capacity was expected. Cyclic adsorption and desorption experiments were performed. A fixed flow of CO_2 was used (0.15 Nl/min), together with a variating flow of air (0.83–0.55 Nl/min) and water (0.97–14.48 g/h corresponding to 2–30 v% in case it is completely evaporated). **Figure 7** reflects the adsorption capacity obtained from the breakthrough curve divided by the adsorption capacity which is expected from the dynamic isotherm obtained in **Figure 4** (more details in **S6**). It can be observed that even in the extreme case where 30 v% water is used, the cyclic adsorption capacity was barely affected by the presence of water. Moreover, it remained constant in consecutive cycles for the different concentrations of water (**Figure S6**). Note that at low relative humidity, a small decrease in capacity was observed, after which the capacity is totally recovered at higher humidity. Further analysis is needed to understand this behavior.

TABLE 1 | Separation factors for different compositions of feed gas.

Composition	α
15 v% CO_2/85 v% CH_4	3.0
30 v% CO_2/70 v% CH_4	4.1
50 v% CO_2/50 v% CH_4	7.3

Effect of Desorption Time on the Cyclic Performance

Lastly, the separation of a dry, synthetic biogas mixture was evaluated. Mixtures containing different concentrations of CH_4 and CO_2 were investigated. Resulting separation factors α for different CO_2/CH_4-mixture compositions are reported in **Table 1**. The separation factor for CO_2 increases with CO_2 concentration. The separation factor for the 30/70 v% CO_2/CH_4 mixture obtained in this work was 4.1, which is higher than the selectivity value of 2.2 reported by Autié Castro et al. (2017) on ZIF-8 powder at 25°C. However, this was slightly lower than the membrane separation factors found in literature. For small, medium and large ZIF-8 particles, a membrane selectivity of 5.2, 5.4, and 5.2 was reported (Gong et al., 2017). It should be noted that the membrane separation factors are the result of both the adsorption and the diffusion selectivity, hence the higher values that can be obtained (Caro, 2016).

Secondly, the separation of a mixture mimicking biogas obtained from household waste streams was tested (60 v% CH_4, 33 v% CO_2, 6 v% air, 1 v% H_2O). As shown in **Figure 8**, CO_2 was adsorbed selectively, with a CO_2/CH_4 separation factor of about 4.0, which was in line with the reported separation factors mentioned above.

CONCLUSION

In this work, a ZIF-8 monolith obtained using the 3D-fiber deposition technique was investigated. The resulting interwoven structure leads to radial diffusion in the structure. When having a difference in size between the inlet and the monolith, the impact of this radial diffusion and mixing could be beneficial. Breakthrough experiments showed that the distribution of the flow was not optimal, as longer breakthrough times were obtained at the outside channels compared to the channels in the center. However, an *in silico* study showed that already after 1 cm in this 3D-printed structure, the flow should already be quite well dispersed, with only minor deviations. The differences observed in the breakthrough experiments were therefore due to defects and heterogeneities in the structure itself.

Although the adsorption capacity of ZIF-8 is limited as compared to other adsorbents (0.09 mmol/g at 15 v% CO_2), the material can be regenerated rapidly and easily in an isothermal way. Using a flow of 10 Nl/min of air, only 6 s were needed to regenerate the material completely in isotherm conditions. Taking into account that high flow rates can be used for the adsorption as well (up to 5 Nl/min without significant effect on the capacity), very fast adsorption/desorption cycles could be obtained. Moreover, it was shown that even with a fully humidified gas stream, the adsorption capacity or the cyclic behavior remained unaffected thanks to the hydrophobic nature of ZIF-8.

Lastly, the separation of a biogas mixture was studied. A separation factor of 4.1 was found for a mixture of 70 v% CH_4–30 v% CO_2, which was higher than the reported value for a ZIF-8 powder.

DATA AVAILABILITY STATEMENT

The raw data supporting the conclusions of this article will be made available by the authors, without undue reservation.

AUTHOR CONTRIBUTIONS

DS and BV carried out the experiments and developed the idea for the manuscript. BV wrote the manuscript with support from JD. JL fabricated the ZIF-8 3D-printed sample. GB and JD helped during discussions about the project. JD supervised the project.

ACKNOWLEDGMENTS

The authors are grateful to VITO for the 3D-printed ZIF-8 material.

SUPPLEMENTARY MATERIAL

The Supplementary Material for this article can be found online at: https://www.frontiersin.org/articles/10.3389/fceng.2020.589686/full#supplementary-material

REFERENCES

Akhtar, F., Andersson, L., Ogunwumi, S., Hedin, N., and Bergström, L. (2014). Structuring adsorbents and catalysts by processing of porous powders. *J. Eur. Ceram. Soc.* 34 (7), 1643–1666. doi:10.1016/j.jeurceramsoc.2014.01.008

Autié Castro, G., de Oliveira Jardim, E., Reguera, E., Vilarrasa-Garcia, E., Rodriguez-Castellon, E., and Cavalcante, C. L., Jr. (2017). CH_4 and CO_2 adsorption study in ZIF-8 and Al-bdc MOFs. *Biol. Chem.* 4, 234–246. doi:10.1021/acs.iecr.7b01809.s001

Avila, P., Montes, M., and Miró, E. E. (2005). Monolithic reactors for environmental applications: a review on preparation technologies. *Chem. Eng. J.* 109 (1), 11–36. doi:10.1016/j.cej.2005.02.025

Caro, J. (2016). "Supported zeolite and MOF molecular sieve membranes: preparation, characterization, application," in *Zeolites and zeolite-like materials* (Amsterdam, The Netherlands: Elsevier). doi:10.1016/B978-0-444-63506-8.00008-2

Claessens, B., Dubois, N., Lefevere, J., Mullens, S., Cousin-Saint-Remi, J., and Denayer, J. F. M. (2020). 3D-Printed ZIF-8 monoliths for biobutanol recovery. *Ind. Eng. Chem. Res.* 59 (18), 8813–8824. doi:10.1021/acs.iecr.0c00453

Couck, S., Cousin-Saint-Remi, J., Van der Perre, S., Baron, G. V., Minas, C., Ruch, P., et al. (2018). 3D-printed SAPO-34 monoliths for gas separation. *Micropor. Mesopor. Mat.* 255, 185–191. doi:10.1016/j.micromeso.2017.07.014

Couck, S., Lefevere, J., Mullens, S., Protasova, L., Meynen, V., Desmet, G., et al. (2017). CO_2, CH_4 and N_2 separation with a 3DFD-printed ZSM-5 monolith. *Chem. Eng. J.* 308, 719–726. doi:10.1016/j.cej.2016.09.046

Coudert, F.-X. (2017). Molecular mechanism of swing effect in zeolitic imidazolate framework ZIF-8: continuous deformation upon adsorption. *Chem. Phys. Chem.* 18 (19), 2732–2738. doi:10.1002/cphc.201700463

Fairen-Jimenez, D., Galvelis, R., Torrisi, A., Gellan, A. D., Wharmby, M. T., Wright, P. A., et al. (2012). Flexibility and swing effect on the adsorption of energy-related gases on ZIF-8: combined experimental and simulation study. *Dalton. Trans.* 41 (35), 10752–10762. doi:10.1039/c2dt30774j

Fairen-Jimenez, D., Moggach, S. A., Wharmby, M. T., Wright, P. A., Parsons, S., and Düren, T. (2011). Opening the gate: framework flexibility in ZIF-8 explored by experiments and simulations. *J. Am. Chem. Soc.* 133 (23), 8900–8902. doi:10.1021/ja202154j

Gong, X., Wang, Y., and Kuang, T. (2017). ZIF-8-based membranes for carbon dioxide capture and separation. *ACS Sustain. Chem. Eng.* 5 (12), 11204–11214. doi:10.1021/acssuschemeng.7b03613

Govender, S., and Friedrich, H. B. (2017). Monoliths: a review of the basics, preparation methods and their relevance to oxidation. *Catalysts* 7 (2), 13–27. doi:10.3390/catal7020062

Hasan, F. A., Xiao, P., Singh, R. K., and Webley, P. A. (2013). Zeolite monoliths with hierarchical designed pore network structure: synthesis and performance. *Chem. Eng. J.* 223, 48–58. doi:10.1016/j.cej.2013.02.100

Huang, H., Zhang, W., Liu, D., Liu, B., Chen, G., and Zhong, C. (2011). Effect of temperature on gas adsorption and separation in ZIF-8: a combined experimental and molecular simulation study. *Chem. Eng. Sci.* 66 (23), 6297–6305. doi:10.1016/j.ces.2011.09.009

Küsgens, P., Rose, M., Senkovska, I., Fröde, H., Henschel, A., Siegle, S., et al. (2009). Characterization of metal-organic frameworks by water adsorption. *Micropor. Mesopor. Mat.* 120 (3), 325–330. doi:10.1016/j.micromeso.2008.11.020

Lee, J.-Y., An, J., and Chua, C. K. (2017). Fundamentals and applications of 3D printing for novel materials. *Appl. Mater. Today.* 7, 120–133. doi:10.1016/j.apmt.2017.02.004

Lefevere, J., Claessens, B., Mullens, S., Baron, G., Cousin-Saint-Remi, J., and Denayer, J. F. M. (2019). 3D-printed zeolitic imidazolate framework structures for adsorptive separations. *ACS Appl. Nano Mater.* 2 (8), 4991–4999. doi:10.1021/acsanm.9b00934

McEwen, J., Hayman, J.-D., and Ozgur Yazaydin, A. (2013). A comparative study of CO_2, CH_4 and N_2 adsorption in ZIF-8, Zeolite-13X and BPL activated carbon. *Chem. Phys.* 412, 72–76. doi:10.1016/j.chemphys.2012.12.012

Middelkoop, V., Coenen, K., Schalck, J., Van Sint Annaland, M., and Gallucci, F. (2019). 3D printed versus spherical adsorbents for gas sweetening. *Chem. Eng. J.* 357, 309–319. doi:10.1016/j.cej.2018.09.130

Park, K. S., Ni, Z., Côté, A. P., Choi, J. Y., Huang, R., Uribe-Romo, F. J., et al. (2006). Exceptional chemical and thermal stability of zeolitic imidazolate frameworks. *Proc. Natl. Acad. Sci. U.S.A.* 103 (27), 10186–10191. doi:10.1073/pnas.0602439103

Regufe, M. J., Ferreira, A. F. P., Loureiro, J. M., Rodrigues, A., and Ribeiro, A. M. (2019). Electrical conductive 3D-printed monolith adsorbent for CO_2 capture. *Micropor. Mesopor. Mat.* 278, 403–413. doi:10.1016/j.micromeso.2019.01.009

Rezaei, F., and Grahn, M. (2012). Thermal management of structured adsorbents in CO_2 capture processes. *Ind. Eng. Chem. Res.* 51 (10), 4025–4034. doi:10.1021/ie201057p

Rezaei, F., and Webley, P. (2009). Optimum structured adsorbents for gas separation processes. *Chem. Eng. Sci.*, 64 (24), 5182–5191. doi:10.1016/j.ces.2009.08.029

Rezaei, F., and Webley, P. (2010). Structured adsorbents in gas separation processes. *Separ. Purif. Technol.* 70 (3), 243–256. doi:10.1016/j.seppur.2009.10.004

Ruiz-Morales, J. C., Tarancón, A., Canales-Vázquez, J., Méndez-Ramos, J., Hernández-Afonso, L., Acosta-Mora, P., et al. (2017). Three dimensional printing of components and functional devices for energy and environmental applications. *Energy Environ. Sci.* 10 (4), 846–859. doi:10.1039/c6ee03526d

Tanaka, S., Fujita, K., Miyake, Y., Miyamoto, M., Hasegawa, Y., Makino, T., et al. (2015). Adsorption and diffusion phenomena in crystal size engineered ZIF-8 MOF. *J. Phys. Chem. C.* 119 (51), 28430–28439. doi:10.1021/acs.jpcc.5b09520

Thakkar, H., Lawson, S., Rownaghi, A. A., and Rezaei, F. (2018). Development of 3D-printed polymer-zeolite composite monoliths for gas separation. *Chem. Eng. J.* 348, 109–116. doi:10.1016/j.cej.2018.04.178

Venna, S. R., and Carreon, M. A. (2010). Highly permeable zeolite imidazolate framework-8 membranes for CO_2/CH_4 Separation. *J. Am. Chem. Soc.* 132 (1), 76–78. doi:10.1021/ja909263x

Verougstraete, B., Martín-Calvo, A., Van der Perre, S., Baron, G., Finsy, V., and Denayer, J. F. M. (2020). A new honeycomb carbon monolith for CO_2 capture by rapid temperature swing adsorption using steam regeneration. *Chem. Eng. J.* 383, 123075. doi:10.1016/j.cej.2019.123075

Williams, J. L. (2001). Monolith structures, materials, properties and uses. *Catal. Today.* 69 (1–4), 3–9. doi:10.1016/s0920-5861(01)00348-0

Zhang, Z., Xian, S., Xi, H., Wang, H., and Li, Z. (2011). Improvement of CO_2 adsorption on ZIF-8 crystals modified by enhancing basicity of surface. *Chem. Eng. Sci.* 66 (20), 4878–4888. doi:10.1016/j.ces.2011.06.051

Conflict of Interest: The authors declare that the research was conducted in the absence of any commercial or financial relationships that could be construed as a potential conflict of interest.